JOURNAL OF NATURAL PRODUCTS

ARTICLE

pubs.acs.org/jnp

Importance of Solvation in Understanding the Chiroptical Spectra of Natural Products in Solution Phase: Garcinia Acid Dimethyl Ester

Prasad L. Polavarapu,*[,†] Giovanni Scalmani,[‡] Edward K. Hawkins,[†] Carmelo Rizzo,[†] Neha Jeirath,[†] Ibrahim Ibnusaud,[§] Deenamma Habel,[§] Divya Sadasivan Nair,[§] and Simimole Haleema[§]

[†]Department of Chemistry, Vanderbilt University, Nashville, Tennessee 37235, United States

[‡]Gaussian, Inc., 340 Quinnipiac Street, Building 40, Wallingford, Connecticut 06492, United States

[§]Institute for Intensive Research In Basic Sciences, Mahatma Gandhi University, P.D. Hills PO, Kottayam, Kerala, India 686 560

Supporting Information

ABSTRACT: The optical rotatory dispersion (ORD), electronic circular dichroism (ECD), and vibrational circular dichroism (VCD) spectra of (+)-garcinia acid dimethyl ester have been measured and analyzed by comparison with the corresponding spectra predicted by quantum chemical methods for (2*S*,3*S*)-garcinia acid dimethyl ester. For solution-phase calculations the recently developed continuous surface charge polarizable continuum model (PCM) has been used. It is found that gas-phase predictions and PCM predictions at the B3LYP/aug-cc-pVDZ level yield nearly mirror-image ECD spectra in the 190−250 nm region for the same absolute configuration and that gas-phase ECD predictions lead to incorrect absolute configuration. At the CAM-B3LYP/aug-cc-pVDZ level, however, gas-phase predictions and PCM predictions of ECD in the 190−250 nm region are not so different, but PCM predictions provide better agreement with the experimental observations. For carbonyl stretching vibrations, the vibrational band positions predicted at the B3LYP/aug-cc-pVDZ level in gas-phase calculations differ significantly from the corresponding experimentally observed band positions, and this discrepancy has also been corrected by the use of PCM. In addition, the solution-phase VCD predictions provided better agreement (with experimental VCD observations) than gas-phase VCD predictions. These observations underscore the importance of including solvent effects in quantum chemical calculations of chiroptical spectroscopic properties.

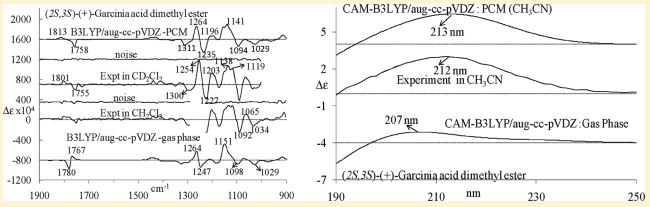

Optically active γ-butyrolactones and related bislactones with various ring appendages are ubiquitous in nature and have attracted much attention[1] in recent years due to their broad biological applications. Functionalized chiral γ-butyrolactones are found in core units of several classes of marketed and potential therapeutic drugs. These classes span[2−9] anti-inflammatory phospholipase A2 inhibitors (Cinatrin class), antineoplastic agents (PKC inhibitors), antihypertensives (vasodilators class), antitumor, antibiotic, and antiarithretic agents, ATP citrate lyase inhibitors, cognition-disorders agents, and antibacterial and antifungal reagents. The organic acids present in the dried rind of the fruit of *Garcinia cambogia* (aka "Malabar tamarind") have been credited[10−13] for the unique regulatory role in fatty acid synthesis, lipogenesis, antiobesity, and weight loss. Later it was revealed[14] that one of the acids responsible for such biological properties was an optically active 2-hydroxycitric acid **1**, which was isolated as garcinia acid **2** [(2*S*,3*S*)-tetrahydro-3-hydroxy-5-oxo-2,3-furandicarboxylic acid]. This molecule and other molecules containing a closely related γ-butyrolactone ring system have been incorporated into a wide range of pharmaceutical preparations and several classes of marketed potential therapeutic drugs. The isolation of 2-hydroxycitric acids including **1** in their natural forms is extremely difficult because of their spontaneous lactonization during (their) isolation due to the presence of a γ-hydroxy group[14] (Scheme 1).

The chiroptical properties of these lactone chromophores are of interest, in view of their prevalence in the pharmaceutical domain. The pharmaceutical action of a compound depends on molecular recognition, which in turn depends on its absolute configuration and conformation. Hence, the absolute configuration of lactones is a matter of great interest. To derive the absolute configuration of lactones, several empirical rules have been formulated over the years.[15−17] These rules, while based on empirical criteria, hold remarkably well on a majority of the lactone chromophores. Nevertheless, consensus is lacking on the generality of these methods in deducing the absolute configuration.[18]

Although **2** and some of its derivatives are known to have important biological functions[14,19a] and antifungal activity,[19b] the chemistry of garcinia acid and its derivatives has not yet been fully explored. The absolute configuration of (+)-garcinia acid has been proposed to be (2*S*,3*S*) (**2**) on the basis of empirical criteria,[20] which was later confirmed via crystal structure determination of its calcium salt.[21] Modern chiroptical spectroscopic analyses have not yet been applied to **2** or its derivatives.

Special Issue: Special Issue in Honor of Koji Nakanishi

Received: July 27, 2010
Published: November 29, 2010

ACS Publications Copyright © 2010 American Chemical Society and American Society of Pharmacognosy

Scheme 1

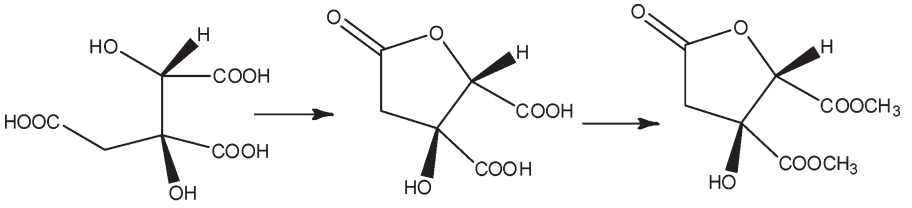

1 2 3

The four chiroptical spectroscopic properties that have gained increased attention[22,23] in recent years include ECD, ORD, VCD, and vibrational Raman optical activity (ROA). The increasing interest in these methods is due to the reliability of their applications to chiral molecular structure determination and the ease with which they can be applied. The availability of commercial instruments made the routine experimental chiroptical spectroscopic measurements feasible, and recent advances in quantum chemical methods[24−27] resulted in achieving reliable predictions of chiroptical properties. Wider access to chiroptical instruments and to quantum chemical software that can calculate chiroptical properties, combined with the availability of faster computers for quantum chemical calculations, made it straightforward to apply chiroptical methods for determining the structures of chiral molecules ranging from small organic molecules to large natural products.

Chiral natural products with different stereochemistries can have very different biological effects. For example two diastereomeric natural products, garcinia acid and hibiscus acid, have different biological functions.[4,19a,28,29] It is essential to establish the relations between chiroptical properties of a natural product and its 3D structure. Carboxylic acids can have hydrogen-bonding interactions with polar solvents such as H_2O or DMSO, rendering the interpretations of observed spectra difficult.[30] However, when the acid groups are converted to esters,[31] such interactions can be avoided and spectroscopic analyses made more conveniently. For this reason, **2** has been converted to its dimethyl ester, **3** (Scheme 1), and used here to explore the chiroptical spectra−structure relations.

Specifically, we investigate if the absolute configuration and predominant conformations of **3** can be determined independently using ECD, ORD, and VCD methods. Since the chemical conversion of **2** to **3** does not involve configurational changes, the absolute configuration of **2** can also be deduced from that of **3**. This is the first investigation of **3** using modern chiroptical methods.

Even in the absence of solvent hydrogen-bonding interactions with solute molecules, solvation can have an important influence on the experimental chiroptical properties. This point became evident from the recent optical rotation measurements[32] of Vaccaro and co-workers in the gas phase using cavity ring down polarimetry,[33] where gas-phase optical rotations were found to be significantly different from solution-phase measurements. Since then, the influence of solvation on chiroptical properties has been gaining attention, and quantum chemical theories are being developed for modeling solvation, even though theoretical modeling of solvation is challenging from a practical point of view. The polarizable continuum model (PCM)[34,35] is by far the most widely used method for studying the influence of solvation on optical rotation,[36] ECD,[37] and ROA[38] spectra. A limited number of PCM investigations on VCD spectra were also reported, especially in the context of VCD induced[39] by a chiral solute in an achiral solvent. However, recently it was found[40] that the PCM, as implemented in the Gaussian 03 program, is not adequate to explain the vibrational absorption (VA) and VCD spectroscopic properties of 6,6′-dibromo-1,1′-binaphthol. This is because some bands in the PCM predicted VA and VCD spectra were shifted to regions where there are no corresponding experimental bands and the comparison with experimental spectra became poorer than that between gas-phase predicted and experimental spectra. Furthermore, two conformers of 6,6′-dibromo-1,1′-binaphthol that are stable in the gas phase (with all real vibrational frequencies) turned out not to be the case in the PCM predictions, where imaginary vibrational frequencies were found. These incorrect predictions of PCM were in part due to discontinuities and approximations in the definition and the implementation of the free energy functional in solution and of the corresponding analytical derivatives. These issues have now been resolved with the introduction of the continuous surface charge PCM[41] as implemented in Gaussian 09.[42] Note that the unsatisfactory results previously obtained[40] for 6,6′-dibromo-1,1′-binaphthol have been rectified[43] by the improvements in the solvent model.[41,42] In the current study, we investigated the solution-phase spectroscopic properties using the recent implementation of PCM.[41,42]

RESULTS AND DISCUSSION

Populations of Conformers. One of eight possible conformations of **3** is shown in Figure 1. The energies of the different B3LYP/aug-cc-pVDZ-optimized conformations are summarized in Table 1, where three different energies are listed: (a) internal energy (IE), which is the energy of the stationary electrons and nuclei; (b) the sum of IE and zero-point energy (ZPE); and (c) Gibbs free energy (FE). To calculate the populations of different conformers in the gas phase, some researchers use IE, while others use FE. The calculation of populations of conformers in solution phase is more complicated because the thermodynamics of solvation includes nonelectrostatic terms (such as cavitation, dispersion, repulsion, and first solvation shell structure effects). In the absence of a clear-cut preference, we chose to consider the sum of IE and ZPE, along with IE and FE separately, for calculating the populations. These populations are also summarized in Table 1. It may be noted that there are no significant differences in the populations derived from these energies obtained in the gas-phase calculation. In the case of populations in CH_3CN and CH_2Cl_2 some differences can be seen among the populations derived from the three energies, but they are not large enough to significantly influence the simulated spectra (*vide infra*). For this reason populations derived from the three

dx.doi.org/10.1021/np100512w |*J. Nat. Prod.* 2011, 74, 321–328

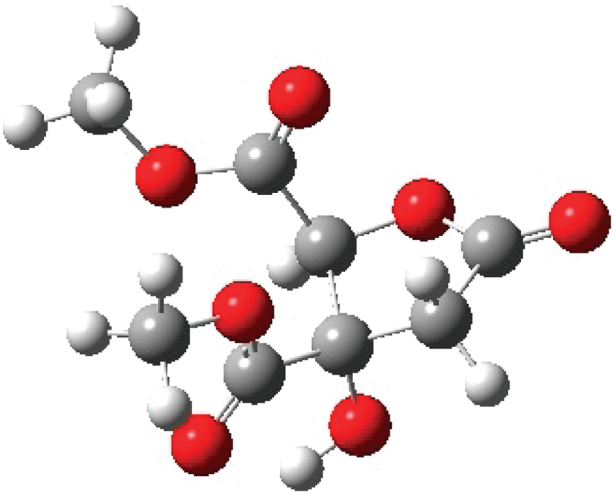

Figure 1. Structure of (2*S*,3*S*)-(+)-garcinia acid dimethyl ester in *cis*−*cis* conformation with positive O−C(=O)−C−C ring puckering angle. Dihedral angles, O=C−C−O and O=C−C−OH, which define the orientations of $COOCH_3$ groups, are used to label the conformations as *cis* (0° ± 30°) or *trans* (180° ± 30°). The *cis*−*cis* conformation shown here has −28° and −12° respectively for the dihedral angles O=C−C−O and O=C−C−OH. The conformations labeled 1−4 (see Table 1) have, respectively, *cis*−*cis*, *trans*−*cis*, *cis*−*trans*, and *trans*−*trans* orientations of dihedral angles O=C−C−O and O=C−C−OH. The same order applies for conformations 5−8. The O−C(=O)−C−C ring puckering angle in conformers 1−4 is positive, while that in conformers 5−8 is negative.

energies are averaged and used in deriving the averaged population-weighted predicted spectra.

Electronic Absorption and Circular Dichroism Spectra. The 25 electronic transitions used for calculating the EA and ECD spectra at the B3LYP/aug-cc-pVDZ level span the range 125−250 nm. The predicted spectra for individual conformers and the population-weighted spectra are provided as Supporting Information. The averaged population-weighted gas-phase predicted ECD spectrum of (2*S*,3*S*)-garcinia acid dimethyl ester exhibits three prominent Cotton effects (CE) (negative at 226 nm, positive at 204 and 167 nm), while the EA spectrum exhibits one strong absorption band at 172 nm and a weak broad absorption band spanning ∼200−230 nm with no well-defined peak position. The experimental spectra could be measured only to a short wavelength limit of 190 nm. Thus the only bands of interest in the predicted spectra for comparison with the experimental spectra are those in the 190−250 nm region. The comparison between the experimental spectra of (+)-garcinia acid dimethyl ester and predicted spectra of (2*S*,3*S*)-garcinia acid dimethyl ester in the 190−250 nm region is shown in Figure 2. The experimental EA spectrum in CH_3CN shows weak absorption broadly spread out with a plateau in the 208−211 nm range. The experimental ECD spectrum in CH_3CN shows a single positive CE at 212 nm. In the 190−250 nm region, the predicted EA spectrum shows a weak and broadly spread out band starting from ∼200 nm toward longer wavelengths, with no well-defined peak position. It is often the case that the predicted electronic transition wavelengths[44] are higher than the experimentally observed wavelengths, and the predicted bands in such cases have to be blue-shifted. With that assumption, the lowest energy negative CE at 226 nm in the averaged population-weighted spectrum corresponds to the lowest energy experimental positive CE at 212 nm. Since the calculations were done for (2*S*,3*S*)-garcinia acid dimethyl ester and experimental data obtained for (+)-garcinia acid dimethyl ester, the gas-phase calculated ECD spectrum, would predict the (2*R*,3*R*) configuration for (+)-garcinia acid dimethyl ester, which is the opposite of the reported[20,21] absolute configuration. This conclusion will be reversed when the solvent-phase predicted ECD is considered (*vide infra*) as well as when other chiroptical methods are applied to **3** (*vide infra*). Thus, it is necessary to emphasize[45] the need for using more than one spectroscopic method for determining the structures of chiral molecules.

The PCM-predicted EA and ECD spectra for individual conformers at the B3LYP/aug-cc-pVDZ level are provided as Supporting Information. Since there are some differences in the populations derived from different energies (namely, IE, IE+ZPE, and FE), the ECD spectra were also simulated using the populations derived from each of these energies. The comparison among the population-weighted predicted ECD spectra (using populations derived from different energies) is also provided as Supporting Information. Irrespective of the energy used for deriving the populations, the population-weighted spectra appear similar in all these cases. As shown in the Supporting Information, the averaged population-weighted solution-phase predicted ECD spectrum exhibits four prominent CEs (negative at 141 nm, positive at 172 nm, negative at 206 nm, and positive at 231 nm), while the EA spectrum exhibits one strong band at 168 nm and a weak broad band spanning ∼200−230 nm with no well-defined peak position. The experimental spectra in the 190−250 nm region are compared with the averaged population-weighted spectra in Figure 2. The solution-phase predicted results obtained using the PCM reveal significant differences from the gas-phase predicted results (see Figure 2). Most importantly, in the 190−250 nm region, the predicted ECD spectrum obtained with the PCM is a near mirror image, with smaller magnitudes, of that obtained in the gas-phase prediction, both for the same (2*S*,3*S*)-garcinia acid dimethyl ester. The lowest energy positive CE at 231 nm in the spectrum predicted with PCM is correlated to the lowest energy positive CE at 212 nm in the experimental ECD spectrum. As a result, at the B3LYP/aug-cc-pVDZ level, the PCM-ECD calculations predict (2*S*,3*S*) absolute configuration for (+)-garcinia acid dimethyl ester, while gas-phase ECD calculations predict the opposite. This appears to be the first observation where the PCM predictions reversed the sign of the gas-phase predicted ECD spectrum (in the 190−250 nm region) and reversed the absolute configuration inferred from gas-phase predictions. This observation is remarkable for highlighting the importance of solvation on predicted ECD spectra.

Larger exact exchange contributions in density functionals is known to lead to a better agreement between experimental and predicted transition wavelengths and ECD spectra. To verify this for **3**, EA and ECD calculations were also performed with the CAM-B3LYP functional using the same aug-cc-pVDZ basis set. The populations derived from IE at the CAM-B3LYP/aug-cc-pVDZ level are similar to those obtained at the B3LYP/aug-cc-pVDZ level (Table 1). The population-weighted gas-phase and solution-phase predicted spectra at the CAM-B3LYP/aug-cc-pVDZ level are compared to the experimental spectra in Figure 3. Although there is no sign reversal between gas- and solution-phase predicted ECD spectra, it can be seen that the solution-phase predicted ECD spectrum is a near replica of the experimental ECD spectrum, while the gas-phase predicted spectrum shows considerable deviation. The solution-phase predicted

Table 1. Energies[a] and Populations of Optimized Conformers of (2*S*,3*S*)-Garcinia Acid Dimethyl Ester at the B3LYP/aug-cc-pVDZ Level

	energies			populations			
conformer[b]	internal energy (IE)	IE + zero-point energy (ZPE)	free energy (FE)	from IE	from IE + ZPE	from FE	average
			isolated molecule				
1	−837.572222	−837.385997	−837.429076	0.17	0.18	0.16	0.17
2	−837.5731	−837.386815	−837.430000	0.44	0.44	0.42	0.43
3	−837.570186	−837.384121	−837.427383	0.02	0.02	0.03	0.02
4	−837.571887	−837.385625	−837.428879	0.12	0.12	0.13	0.12
5	−837.572406	−837.38604	−837.429408	0.21	0.19	0.22	0.21
6	−837.570639	−837.38445	−837.427887	0.03	0.03	0.04	0.04
7	−837.567497	−837.381442	−837.425016	0.00	0.00	0.00	0.00
8	−837.567664	−837.381684	−837.425692	0.00	0.00	0.00	0.00
			CH_3CN				
1	−837.590257	−837.404373	−837.447309	0.36	0.31	0.20	0.29
2	−837.589546	−837.403899	−837.447345	0.17	0.19	0.21	0.19
3	−837.588951	−837.403043	−837.446245	0.09	0.08	0.06	0.08
4	−837.58814	−837.402476	−837.446355	0.04	0.04	0.07	0.05
5	−837.589647	−837.404014	−837.447515	0.19	0.21	0.25	0.22
6	−837.589403	−837.403719	−837.447279	0.14	0.16	0.19	0.16
7	−837.586738	−837.401078	−837.444949	0.01	0.01	0.02	0.01
8	−837.585721	−837.399969	−837.443622	0.00	0.00	0.00	0.00
			CH_2Cl_2				
1	−837.587766	−837.40178	−837.444632	0.35	0.29	0.16	0.27
2	−837.587307	−837.401533	−837.444884	0.22	0.22	0.20	0.21
3	−837.586278	−837.400312	−837.443517	0.07	0.06	0.05	0.06
4	−837.585967	−837.400204	−837.443944	0.05	0.05	0.07	0.06
5	−837.586992	−837.401361	−837.445128	0.15	0.19	0.27	0.20
6	−837.586952	−837.401289	−837.445045	0.15	0.17	0.24	0.19
7	−837.583799	−837.397993	−837.441642	0.01	0.01	0.01	0.01
8	−837.583163	−837.397289	−837.440732	0.00	0.00	0.00	0.00

[a] Energies are in atomic units. [b] Conformers 1−4 have positive O−C(=O)−C−C ring puckering angle, and 5−8 have negative O−C(=O)−C−C ring puckering angle; the O=C−C−O and O=C−C−OH dihedral angles at the two stereocenters are (*cis,cis*), (*trans,cis*), (*cis,trans*), and (*trans,trans*) for confomers 1−4 (and the same for 5−8).

ECD intensity maximum at 213 nm and band shape match very well with the corresponding experimentally observed ECD (maximum at 212 nm). On the other hand, the gas-phase predicted ECD shape deviates significantly from the experimental ECD shape, and the band maximum (207 nm) is blue-shifted. It appears, therefore, that the solution-phase predictions for **3** provide better agreement with the corresponding experimental observations than gas-phase predictions do. It should be emphasized, however, that the observed ECD for **3** is of very small magnitude. Although the reversals of predicted signs can occur in such cases with some changes in theoretical parameters, the better performance of the PCM model for **3** with both CAM-B3LYP and B3LYP functionals suggests that the solution-phase ECD calculations are to be preferred over gas-phase calculations for analyzing the experimental observations in solution phase.

Optical Rotatory Dispersion Spectra. The experimental ORD spectra of (+)-garcinia acid dimethyl ester measured in CH_3CN and CH_2Cl_2 solvents are compared to the gas-phase and solution-phase predictions, at the B3LYP/aug-cc-pVDZ level, for (2*S*,3*S*)-garcinia acid dimethyl ester in Figure 4. The gas-phase predicted ORD spectrum is obtained from calculations on a single molecule, while solution-phase predicted ORD spectra were obtained with the PCM using CH_3CN and CH_2Cl_2 separately. All calculations predicted positive specific rotations for (2*S*,3*S*)-garcinia acid dimethyl ester at all six wavelengths investigated, with increasing magnitudes at shorter wavelengths. The same trend with positive specific rotations is observed in the experimental ORD spectra of (+)-garcinia acid dimethyl ester.

Since the use of the CAM-B3LYP functional led to better agreement between predicted and experimental ECD spectra, we repeated the ORD calculations at the CAM-B3LYP/aug-cc-pVDZ level. These ORD predictions, however, are identical to those at the B3LYP/aug-cc-pVDZ level and are therefore presented as Supporting Information.

Thus, the predicted ORD spectra, regardless of the nature of calculations (gas phase vs solution phase and B3LYP vs CAM-B3LYP), concur with the known[20,21] absolute configuration of **3**. The fact that gas-phase ECD calculations at the B3LYP/aug-cc-pVDZ level did not predict the known absolute configuration, but gas-phase ORD calculations at the same level did predict the known absolute configuration, indicates the need for investigating ORD and ECD simultaneously,[46] rather than individually. Moreover, since ORD can be viewed as a Kramers−Kronig transform of the entire ECD spectrum, the ORD spectrum in the visible region must not have been dominated by the contribution from lowest energy ECD bands.

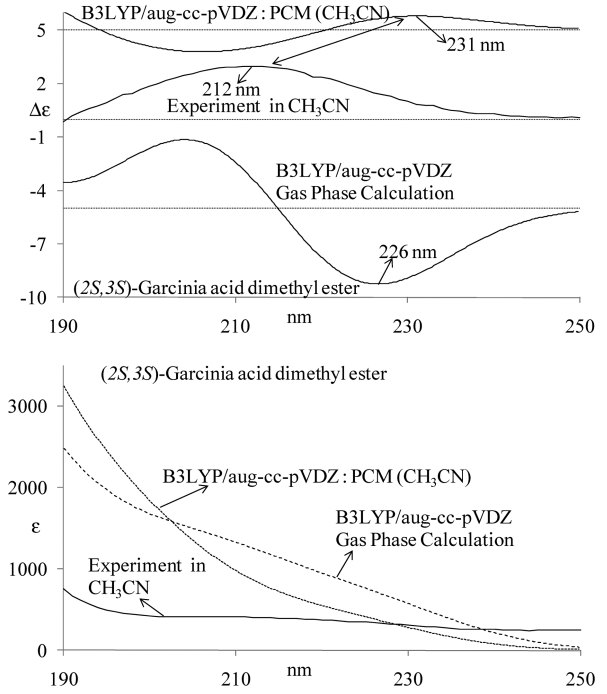

Figure 2. EA (bottom panel) and ECD (top panel) spectra of (2*S*,3*S*)-(+)-garcinia acid dimethyl ester. Gas-phase results represent calculations for a single molecule, and PCM (CH_3CN) results represent PCM calculations for solvated molecule in acetonitrile solvent, both at the B3LYP-aug-cc-pVDZ level.

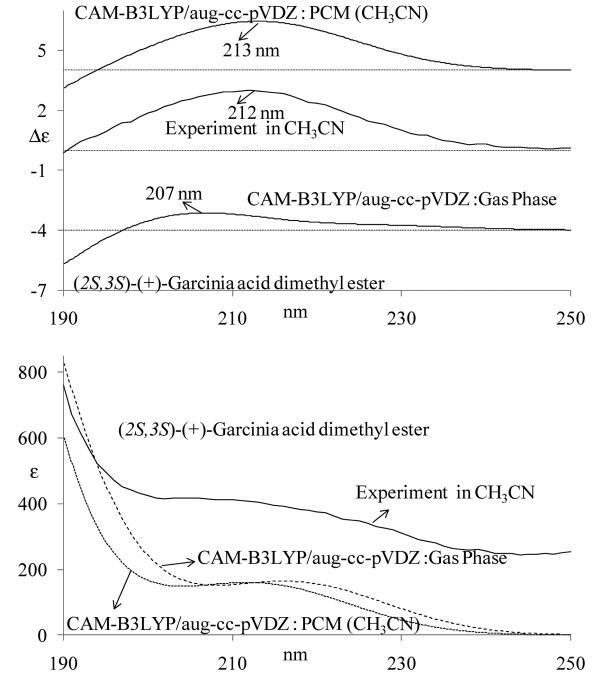

Figure 3. EA (bottom panel) and ECD (top panel) spectra of (2*S*,3*S*)-(+)-garcinia acid dimethyl ester. Gas-phase results represent calculations for a single molecule, and PCM (CH_3CN) results represent PCM calculations for a solvated molecule in acetonitrile solvent, both at the CAM-B3LYP-aug-cc-pVDZ level.

Wiberg and co-workers[47] reported that among the optical rotations measured in different solvents for 2-chloropropionitrile, those in CH_3CN are closer to the gas-phase measured

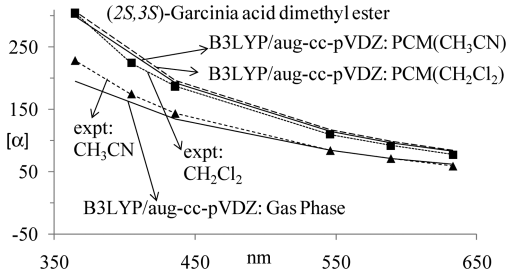

Figure 4. ORD spectra of (2*S*,3*S*)-(+)-garcinia acid dimethyl ester. Gas-phase results represent calculations for a single molecule, and PCM results represent PCM calculations for a solvated molecule in CH_3CN or CH_2Cl_2, both at the B3LYP-aug-cc-pVDZ level.

values. This observation cannot be verified for **3**, as the experimental ORD measurements could not be made in the gas phase. As far as the PCM model is concerned, the predicted ORD spectra are identical in CH_3CN and CH_2Cl_2, and they both differ slightly from gas-phase predicted ORD spectra.

Vibrational Absorption and Circular Dichroism Spectra. The predicted VA and VCD spectra, at the B3LYP/aug-cc-pVDZ level, for individual conformers in both the gas- and solution-phase calculations are provided as the Supporting Information. The population-weighted VCD spectra in the solution-phase calculation, with populations obtained separately from IE, IE+ZPE, and FE, are also compared to each other (see Supporting Information), and no significant differences are apparent. For this reason, these separate populations are averaged to generate averaged population-weighted spectra and used to compare with the experimental spectra. The experimental VA and VCD spectra of (+)-garcinia acid dimethyl ester are compared to the averaged population-weighted spectra of (2*S*,3*S*)-garcinia acid dimethyl ester in Figure 5. In the carbonyl stretching region, the predicted gas-phase absorption spectrum shows two strong bands at 1860 and 1777 cm^{-1}, but the corresponding experimental bands are located at 1805 and 1751 cm^{-1}, indicating a significant mismatch between experimental and gas-phase predicted vibrational band positions. Accordingly, there is also a mismatch between the experimental and gas-phase predicted VCD band positions in the carbonyl stretching region. While the two experimental absorption bands at 1805 and 1751 cm^{-1} are associated with very weak positive and negative VCD bands, respectively, the predicted gas-phase absorption band at 1860 cm^{-1} exhibits no significant VCD and that at 1777 cm^{-1} exhibits a bisignate VCD couplet (negative band at 1780 and weak positive band at 1767 cm^{-1}). These discrepancies are minimized in the computed solution-phase spectra, where the two strong absorption bands predicted at 1816 and 1757 cm^{-1} correlate well with the experimental absorption bands at 1805 and 1751 cm^{-1}. The VCD intensities associated with the solution-phase predicted absorption bands at 1816 and 1757 cm^{-1}, positive for the former and negative for the latter, are both very weak. The corresponding experimental VCD band intensities at 1801 and 1755 cm^{-1} are also very weak. It can be clearly seen that the solution-phase predicted VA and VCD spectra are in much better agreement, than are gas-phase predicted spectra, with the corresponding experimental spectra in the carbonyl stretching region, emphasizing the importance of solvation in predicting VA and VCD spectra of chiral molecules. In the ~1300−900 cm^{-1} region the experimental VCD spectrum compares better with the solution-phase predicted spectrum than with the gas-phase predicted spectrum. The missing

dx.doi.org/10.1021/np100512w |*J. Nat. Prod.* 2011, 74, 321–328

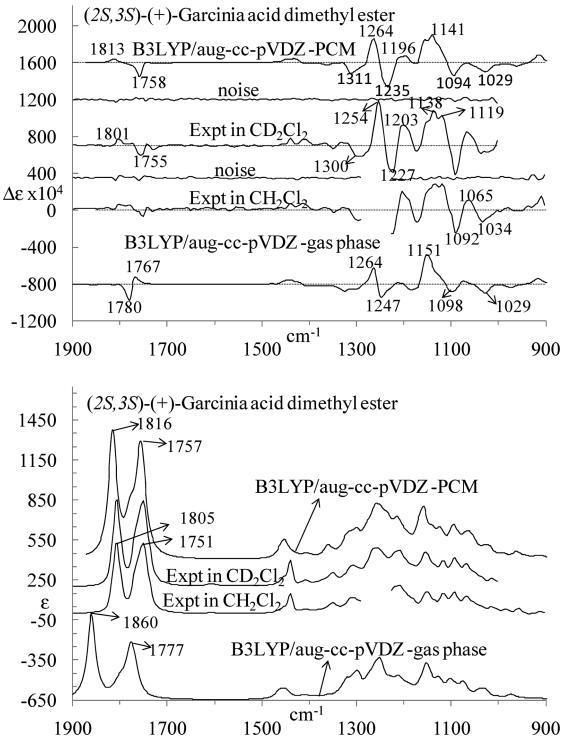

Figure 5. VA (bottom panel) and VCD (top panel) spectra of (2*S*,3*S*)-(+)-garcinia acid dimethyl ester. Gas-phase results represent calculations for a single molecule, and PCM results represent PCM calculations for solution-phase in CH_2Cl_2, both at the B3LYP-aug-cc-pVDZ level. The spectra are offset for clarity. The traces labeled "noise" represent the noise level in experimental VCD spectra.

~1290−1230 cm^{-1} region in the experimental VCD spectrum measured in CH_2Cl_2 can be seen in the experimental VCD spectrum measured in CD_2Cl_2. A weak negative VCD at ~1300 cm^{-1}, strong positive VCD at 1254 cm^{-1}, and negative VCD at 1227 cm^{-1} are present in this region, and these three bands are reproduced in the predicted spectra (more pleasingly in solution-phase predicted spectrum than in gas-phase predicted spectrum). In the 1220−900 cm^{-1} region, the experimental VCD spectrum exhibits a positive band at 1203 cm^{-1}, a broad envelope of three positive bands with resolved central component at 1138 cm^{-1}, a weak negative band at 1092 cm^{-1}, a positive band at 1065 cm^{-1}, and a weak negative band at 1034 cm^{-1}. These features are better reflected in the solution-phase predicted VCD spectrum than in the gas-phase predicted VCD spectrum. This is because the positive band at 1203 cm^{-1} and adjacent broad envelope of positive VCD bands have counterparts in the solution-phase predicted VCD spectrum at 1196 and 1141 cm^{-1}, respectively. In the gas-phase predicted VCD spectrum, the former is not apparent and the latter appears as a sharper positive band at 1151 cm^{-1}. Thus the overall agreement between predicted and experimental spectra is improved in PCM calculations, over that in gas-phase calculations, for both VA and VCD spectra. This observation also emphasizes the importance of solvation in interpreting the VA and VCD spectra.

It is useful to point out that there are numerous VCD reports where gas-phase predictions were compared with solution-phase experimental spectra and significant mismatches between predicted and experimental band positions were apparent in the mid-infrared region. It is hoped that the current observations on **3** will encourage the incorporation of solvent effects in VCD predictions.

CONCLUSIONS

The analysis of ECD, ORD, and VCD data confirms the absolute configuration of garcinia acid dimethyl ester as (2*S*,3*S*)-(+). Since chemical conversion of garcinia acid to its ester does not influence the absolute configuration, this conclusion can be extrapolated to the parent acid as (2*S*,3*S*)-(+)-garcinia acid. Thus, the present study confirms the absolute configurations of both garcinia acid and its dimethyl ester. Furhermore, this study reveals that the garcinia acid dimethyl ester molecule adopts eight different conformations, four of which have nearly 20% population each. The solvation influence in CH_3CN and CH_2Cl_2 solutions is seen to be significant. In particular, modeling of solvent effect by means of the PCM has turned out to be important for the prediction of absolute configuration of garcinia acid dimethyl ester from ECD spectra. The experimental VA and VCD spectra of garcinia acid dimethyl ester have also been reproduced better when solvent effects are introduced using the PCM.

EXPERIMENTAL SECTION

General Experimental Procedures. Garcinia acid was isolated from fresh dried rind collected locally following the reported procedure[48] and was esterified with excess diazomethane to afford garcinia acid dimethyl ester as previously reported.[14]

The optical rotations at six discrete wavelengths (633, 589, 546, 436, 405, 365 nm) were measured with a 0.5 dm cell using an Autopol IV polarimeter. ORD measurements were obtained at a concentration of 2.8 mg/mL in CH_3CN and 3.4 mg/mL in CH_2Cl_2. The EA and ECD spectra were recorded on a Jasco J720 spectrometer, at a concentration of 2.8 mg/mL in CH_3CN using a 0.01 cm path length quartz cell. The solvent spectrum has been subtracted from the experimental ECD spectrum of the sample solution. The CH_2Cl_2 absorption prevents ECD measurements below ~230 nm, and for this reason this solvent could not be used for ECD measurements on **3**.

The VA and VCD spectra were recorded in the 2000−900 cm^{-1} region using a commercial Fourier transform VCD spectrometer, which has been modified and recently aligned to reduce the level of artifacts. The VCD spectra were recorded with a one-hour data collection time at 8 cm^{-1} resolution. The infrared absorptions of CH_3CN and CD_3CN interfere with VCD measurements in large portions of the mid infrared region. The infrared absorptions of CH_2Cl_2 and CD_2Cl_2 interfere only in smaller portions of the mid infrared range. For these reasons VA and VCD spectra were measured in CH_2Cl_2 and CD_2Cl_2 at a concentration of 3 mg/100 μL. The samples were held in a 100 μm fixed path length cell with BaF_2 windows. In the VA spectrum, the solvent absorption was subtracted. The region ~1290−1230 cm^{-1} has been excluded for the spectra measured in CH_2Cl_2 due to interference from CH_2Cl_2 absorption. The region ~1000−900 cm^{-1} has been excluded for the spectra measured in CD_2Cl_2 due to interference from CD_2Cl_2 absorption. The solvent VCD spectrum was subtracted from that of the sample solution.

Computational Details. All calculations were performed for (2*S*,3*S*)-garcinia acid dimethyl ester (see Figure 1) using both the B3LYP[49] and the CAM-B3LYP[50] functionals and the aug-cc-pVDZ basis set.[51] At each of the two stereogenic centers, the $COOCH_3$ group can be oriented in two different ways (by flipping it 180° around the C_{ring}−C bond at the stereocenters). At the C-3 stereocenter with OH and $COOCH_3$ groups attached, these orientations correspond to intramolecular hydrogen bonding between the hydroxy hydrogen atom of the O−H group and oxygen of the C═O group or between

the hydroxy hydrogen atom of the O−H group and oxygen of the OCH_3 group. Two different puckering angles are possible for the furan ring. Thus, a total of eight conformations were investigated. VA, VCD, EA, ECD, and ORD properties have been calculated at the same level for all eight conformations at their respective optimized geometries as obtained using the B3LYP functional. The geometries have not been optimized using the CAM-B3LYP functional, as the latter differs from B3LYP mainly in the description of the tails of the electronic density, and that is not likely to affect the molecular geometry in a significant way. Calculations were performed on the isolated molecule, to model the gas phase, and also on the solvated molecule using the most recent implementation of the PCM[41] model, to simulate the solution phase. The Gaussian 09 program[42] has been used for the present calculations.

The theoretical VA and VCD spectra were simulated with Lorentzian band shapes of 10 cm^{-1} half-width at half-peak height. The predicted vibrational frequencies are normally higher than the corresponding experimental vibrational frequencies, and therefore the calculated frequencies are usually scaled[52] when smaller basis sets are employed. No such scaling has been used for the vibrational frequencies obtained with the aug-cc-pVDZ basis set.

The theoretical EA and ECD spectra were simulated from the first 25 singlet → singlet electronic transitions using Gaussian band shapes and 15 nm half-width at 1/e of peak height. Rotational strength values, calculated in the velocity representation, have been used for the ECD spectral simulations. The EA spectral intensities are derived from dimensionless oscillator strengths. The predicted electronic transition energies provided by the B3LYP functional are generally lower[44] than the corresponding experimental values, but a uniform scaling factor may not be satisfactory for all electronic transition energies. Therefore the predicted transition wavelengths were not scaled, but the possibility of longer wavelengths for the predicted EA and ECD bands should be kept in mind in comparing the predicted and experimental spectra. Indeed, the transition wavelengths predicted at the CAM-B3LYP/aug-cc-pVDZ level are in better agreement with experiment. This is consistent with the better description of the tails of the electronic density provided by the CAM-B3LYP functional, which leads to a more accurate description of the excited states that are generally characterized by a less compact electron density.

■ ASSOCIATED CONTENT

Supporting Information. Individual conformer spectra of (2*S*,3*S*)-garcinia acid dimethyl ester, for ECD as well as VCD, in both the gas-phase and solution-phase calculations, a comparison of population-weighted spectra (with populations derived separately from internal energy, internal energy plus zero-point energy, and free energy), ^1H and ^{13}C NMR spectra of (+)-garcinia acid dimethyl ester, and a table of NMR chemical shifts are provided. This material is available free of charge via the Internet at http://pubs.acs.org.

■ AUTHOR INFORMATION

Corresponding Author

*E-mail: Prasad.L.Polavarapu@vanderbilt.edu. Phone: (615) 322-2836. Fax: (615) 322-4936.

■ ACKNOWLEDGMENT

P.L.P. and G.S. would like to thank Dr. James R. Cheeseman for PCM calculations on 6,6′-dibromo-1,1′-binaphthol with the Gaussian 09 program and for helpful discussions and insight on the interpretation of the computed ECD, ORD, and VCD spectra. Assistance from Dr. G. Shanmugam in recording the VCD spectra and NSF funding (CHE-0804301) are gratefully acknowledged. Some of the calculations were carried out at National Center for Supercomputing Applications under grant number CHE090061. E.K.H. was supported by predoctoral traineeships T32 ES07028. I.I., S.H., and D.S.N. would like to acknowledge the Department of Science and Technology, Govt. of India, New Delhi, for financial assistance (Project No. SR/S1/OC/54-2007).

■ DEDICATION

This paper is dedicated to Dr. Koji Nakanishi of Columbia University for his pioneering work on bioactive natural products.

■ REFERENCES

(1) Varugese, S.; Thomas, S.; Haleema, S.; Thomas, T. P.; Ibnusaud, I. *Tetrahedron Lett.* **2007**, *48*, 8209–8212.
(2) Sullivan, A. C. Effect of (−)-hydroxycitrate on lipid metabolism. In *Modification of Lipid Metabolism*; Perks, E. G., Witting, L., Eds.; Academic Press: New York, 1984; pp 143−174.
(3) Yoshida, T. European Patent 405864; 19910102, 1989, Japan Patent 91108490; 19910508, 1989.
(4) Jena, B. S.; Jayaprakasha, G. K.; Singh, R. P.; Sakariah, K. K. *J. Agric. Food Chem.* **2002**, *50*, 10–22.
(5) Sullivan, A. C.; Hamilton, J. G.; Miller, O. N.; Wheatley, V. R. *Arch. Biochem. Biophys.* **1972**, *150*, 183–190.
(6) Sullivan, A. C.; Triscari, J.; Hamilton, J. G.; Miller, O. N.; Wheatley, V. R. *Lipids* **1974**, *9*, 121–128.
(7) (a) Wakat, D. U.S. Patent 6054128, 2000. (b) Drahl, C. *Chem. Eng. News* **2008**, *86*, 35–36.
(8) Tomi, H.; Tamura, K. B. Japan Patent 10004939A2, 1998.
(9) Majeed, M.; Badmaev, V.; Rajendran, R. U.S. Patent 5783603, 1998.
(10) Wielinga, P. Y.; Wachters-Hagedoorn, R. E.; Bouter, B.; van Dijk, T. H.; Stellaard, F.; Nieuwenhuizen, A. G.; Verkade, H. J.; Scheurink, A. J. W. *Am. J. Physiol. Gastrointest. Liver Physiol.* **2005**, *288*, G1144–G1149.
(11) Mackeen, M. M.; Ali, A. M.; Lajis, N. H.; Kawazu, K.; Kikuzaki, H.; Nakatani, N. *Z. Naturforsch.* **2002**, *57*, 291–295.
(12) Heymsfield, S. B.; Allison, D. B.; Vasselli, J. R.; Pietobelli, D. G.; Nunthe, C. *J. Am. Med. Assoc.* **1998**, *280*, 1596–1600.
(13) Ramos, R. R.; Saenz, F. J.; Alarcon, A. *Invest. Med. Int.* **1996**, *22*, 97–100.
(14) Ibnusaud, I.; Thomas, P. T. R.; Rani, R. N.; Sasi, P. V.; Bena, T.; Hisham, A. *Tetrahedron* **2002**, *58*, 4887–892.
(15) Forzato, C.; Nitti, P.; Pitacco, G. *Tetrahedron* **1997**, *8*, 4104–4110.
(16) Beecham, A. F. *Tetrahedron Lett.* **1968**, *3591*, 3594.
(17) Mathieson, A. M. *Tetrahedron Lett.* **1963**, *81*, 84.
(18) Stončius, S.; Berg, U.; Butkus, E. *Tetrahedron: Asymmetry* **2004**, *15*, 2405–2413.
(19) (a) Yamada, T.; Hida, H.; Yamada, Y. *Appl. Microbiol. Biotechnol.* **2007**, *75*, 977–982. (b) Mackeena, M. M.; Ali, A. M.; Lajis, N. H.; Kawazu, K.; Kikuzaki, H.; Nakatani, N. *J. Biosci.* **2002**, *57*, 291–295.
(20) Boll, P. M.; Sorensen, E.; Balieu, E. *Acta Chem. Scand.* **1969**, *23*, 286–293.
(21) Glusker, J. P.; Minkin, J. A.; Casciato, C. A. *Acta Crystallogr.* **1971**, *B27*, 1284–1293.
(22) Barron, L. D.; Buckingham, A. D. *Chem. Phys. Lett.* **2010**, *492*, 199–213.
(23) Autschbach, J. *Chirality* **2009**, *21*, No. E116−E152.
(24) Pecul, M.; Ruud, K. *Adv. Quantum Chem.* **2005**, *50*, 185–212.
(25) Autschbach, J. *Comput. Lett.* **2007**, *3*, 131–150.
(26) Devlin, F. J.; Stephens, P. J.; Cheeseman, J. R.; Frisch, M. J. *J. Am. Chem. Soc.* **1996**, *118*, 6327–6328.
(27) Ruud, K.; Thorvaldsen, A. J. *Chirality* **2009**, *21*, No. E54−E67.

(28) Yamada, T.; Hida, H.; Yamada, Y. *Actinomycetologica* **2007**, *21*, 40–45.
(29) Hida, H.; Yamada, T.; Yamada, Y. *Appl. Microbiol. Biotechnol.* **2007**, *73*, 1387–1393.
(30) He, J.; Polavarapu, P. L. *J. Chem. Theory Comput.* **2005**, *1*, 506–514.
(31) He, J.; Wang, F.; Polavarapu, P. L. *Chirality* **2005**, *17*, S1–S8.
(32) Wilson, S. M.; Wiberg, K. B.; Cheeseman, J. R.; Frisch, M. J.; Vaccaro, P. H. *J. Phys. Chem. A* **2005**, *109*, 11752–11764.
(33) Mueller, T.; Wiberg, K. B.; Vaccaro, P. H. *J. Phys. Chem. A* **2000**, *104*, 5959–5968.
(34) Tomasi, J.; Mennucci, B.; Cammi, R. *Chem. Rev.* **2005**, *105*, 2999–3094.
(35) Cossi, M.; Scalmani, G.; Rega, N.; Barone, V. *J. Chem. Phys.* **2002**, *117*, 43–54.
(36) Mennucci, B.; Tomasi, J.; Cammi, R.; Cheeseman, J. R.; Frisch, M. J.; Devlin, F. J.; Gabriel, S.; Stephens, P. J. *J. Phys. Chem.* **2002**, *106*, 6102–6113.
(37) Pecul, M.; Marchesan, D.; Ruud, K.; Coriani, S. *J. Chem. Phys.* **2005**, *122*, No. 024106.
(38) Pecul, M.; Lamparska, E.; Cappelli, C.; Frediani, L.; Ruud, K. *J. Phys. Chem. A* **2006**, *110*, 2807–2815.
(39) Debie, E.; Jaspers, L.; Bultinck, P.; Herrebout, W.; Vander Veken, B. *Phys. Chem. Chem. Phys.* **2008**, *10*, 3498–3508.
(40) Polavarapu, P. L.; Jeirath, N.; Walia, S. *J. Phys. Chem. A* **2009**, *113*, 5423–5431.
(41) Scalmani, G.; Frisch, M. J. *J. Chem. Phys.* **2010**, *132*, 114110–114124.
(42) Frisch, M. J.; Trucks, G. W.; Schlegel, H. B.; Scuseria, G. E.; Robb, M. A.; Cheeseman, J. R.; Scalmani, G.; Barone, V.; Mennucci, B.; Petersson, G. A.; Nakatsuji, H.; Caricato, M.; Li, X.; Hratchian, H. P.; Izmaylov, A. F.; Bloino, J.; Zheng, G.; Sonnenberg, J. L.; Hada, M.; Ehara, M.; Toyota, K.; Fukuda, R.; Hasegawa, J.; Ishida, M.; Nakajima, T.; Honda, Y.; Kitao, O.; Nakai, H.; Vreven, T.; Montgomery, J. A., Jr.; Peralta, J. E.; Ogliaro, F.; Bearpark, M.; Heyd, J. J.; Brothers, E.; Kudin, K. N.; Staroverov, V. N.; Kobayashi, R.; Normand, J.; Raghavachari, K.; Rendell, A.; Burant, J. C.; Iyengar, S. S.; Tomasi, J.; Cossi, M.; Rega, N.; Millam, J. M.; Klene, M.; Knox, J. E.; Cross, J. B.; Bakken, V.; Adamo, C.; Jaramillo, J.; Gomperts, R.; Stratmann, R. E.; Yazyev, O.; Austin, A. J.; Cammi, R.; Pomelli, C.; Ochterski, J. W.; Martin, R. L.; Morokuma, K.; Zakrzewski, V. G.; Voth, G. A.; Salvador, P.; Dannenberg, J. J.; Dapprich, S.; Daniels, A. D.; Farkas, Ö.; Foresman, J. B.; Ortiz, J. V.; Cioslowski, J.; Fox, D. J. *Gaussian 09, Revision A.02*; Gaussian, Inc.: Wallingford, CT, 2009.
(43) Cheeseman, J. Private communication. The VA and VCD spectra predicted for the three conformers of 6,6′-dibromo-1,1′-binaphthol with PCM implemented in the Gaussian 09 program did not contain misbehaved band shifts or imaginary frequencies.
(44) Caricato, M.; Trucks, G. W.; Frisch, M. J.; Wiberg, K. B. *J. Chem. Theor. Comput.* **2010**, *6*, 370–383.
(45) Polavarapu, P. L. *Chirality* **2008**, *20*, 664–72.
(46) Polavarapu, P. L. *Chirality* **2006**, *18*, 348–356.
(47) Wiberg, K. B.; Wang, Y.; Wilson, S. M.; Vaccaro, P. H.; Cheeseman, J. R. *J. Phys. Chem. A* **2005**, *109*, 3448–3453.
(48) Ibnusaud, I.; Puthiaparampil, T. T.; Thomas, B. U.S. Patent 6147228, 2000.
(49) Becke, A. D. *J. Chem. Phys.* **1993**, *98*, 5648–5652.
(50) Yanai, T.; Tew, D. P.; Handy, N. C. *Chem. Phys. Lett.* **2004**, *393*, 51–57.
(51) Kendall, R. A.; Dunning, T. H., Jr.; Harrison, R. J. *J. Chem. Phys.* **1992**, *96*, 6796–6806.
(52) Wong, M. W. *Chem. Phys. Lett.* **1996**, *256*, 391–399.